Subinertial to interannual transport variations in the Korea Strait and their possible mechanisms

Sang Jin Lyu[1]

Department of Earth, Atmospheric and Planetary Sciences, Massachusetts Institute of Technology, Cambridge, Massachusetts, USA

Kuh Kim

OCEAN Laboratory, Research Institute of Oceanography, School of Earth and Environmental Sciences, Seoul National University, Seoul, South Korea

Received 6 August 2004; revised 14 May 2005; accepted 14 July 2005; published 17 December 2005.

[1] The voltage-derived transport in the Korea Strait from March 1998 to April 2002 reveals various temporal variations such as subinertial, monthly, seasonal, and interannual variations. The driving mechanisms of these temporal variations in the flows through the straits and the mean sea level of the East Sea (Sea of Japan) are investigated using a simple analytical barotropic model. The East Sea is simplified as a flat-bottomed semienclosed basin, and it is forced by the atmospheric pressure, the along-strait wind stress, and the sea level differences along the straits. Despite its simplicity this model explains most variations and helps us understand dominant driving forces on each timescale. At the subinertial periods of 2–10 days the atmospheric pressure dominantly drives the flows into or out of the East Sea due to a Helmholtz resonance, whose period is about 3 days, and the mean sea level cannot respond isostatically. The effects of the atmospheric pressure on the transport variations become weak at long periods because there is enough time for the East Sea to be drained or filled through the strait flows as its mean sea level responds isostatically. On the other hand, the changes in the adjusted sea levels outside the straits of the East Sea cause the pressure gradient forces along the straits and induce most of variations in the strait flows and the mean sea level at the monthly to interannual periods.

Citation: Lyu, S. J., and K. Kim (2005), Subinertial to interannual transport variations in the Korea Strait and their possible mechanisms, *J. Geophys. Res.*, *110*, C12016, doi:10.1029/2004JC002651.

1. Introduction

[2] The East Sea (Sea of Japan, hereinafter referred to as East Sea) is a semienclosed marginal sea connected to the Pacific Ocean and the Sea of Okhotsk through four shallow straits: the Korea (Tsushima), Tsugaru, Soya, and Tartarsky straits (Figure 1). The horizontal length scale of the East Sea is about 1000 km and its mean depth is about 1700 m with a maximum depth of 4000 m. The Tsushima Current flows into the East Sea through the Korea Strait carrying heat and salt from the Western Pacific Ocean, forms the major surface currents in the East Sea and flows out mainly through the Tsugaru and Soya straits [*Moriyasu*, 1972; *Lee et al.*, 2000; *Cho and Kim*, 2000]. Previous estimates of the transport through the Korea Strait vary widely from nearly 0 to 5 Sv (1 Sv = 10^6 m^3 s^{-1}) depending on methods and time [*Yi*, 1966; *Isobe et al.*, 1994]. Recently it has become possible to obtain a reliable estimate of the transport by the implementation of the vessel-mounted ADCP [*Takikawa et al.*, 2005] and the bottom-mounted, trawl-resistant ADCP [*Teague et al.*, 2002]. Moreover, the motion-induced voltage has been measured using the abandoned submarine cable between Pusan, Korea and Hamada, Japan (Figure 1) since March 1998 and the measured voltage showed a close linear relationship with the above two observed transports [*Kim et al.*, 2004]. Continuous measurement of cable voltage revealed large variability in the inflow through the Korea Strait on short-period subinertial to interannual timescales and enabled us to investigate the driving mechanisms of various temporal variations in the flows through the straits of the East Sea.

[3] The driving mechanism of the inflow through the Korea Strait and the outflow through the Tsugaru and Soya straits has been investigated from a mean and steady point of view until now [*Minato and Kimura*, 1980; *Ohshima*, 1994; *Nof*, 1993, 2000]. *Minato and Kimura* [1980] and *Ohshima* [1994] reported that the meridional sea level difference (SLD) between the subtropical and subpolar gyres drives the inflow and the outflow through the straits. On the other hand, *Nof* [1993] proposed that the zonal SLD between the Pacific Ocean and the East Sea causes the

[1]Now at Department of Oceanography, Chonnam National University, Kwangju, South Korea.

0148-0227/05/2004JC002651$09.00

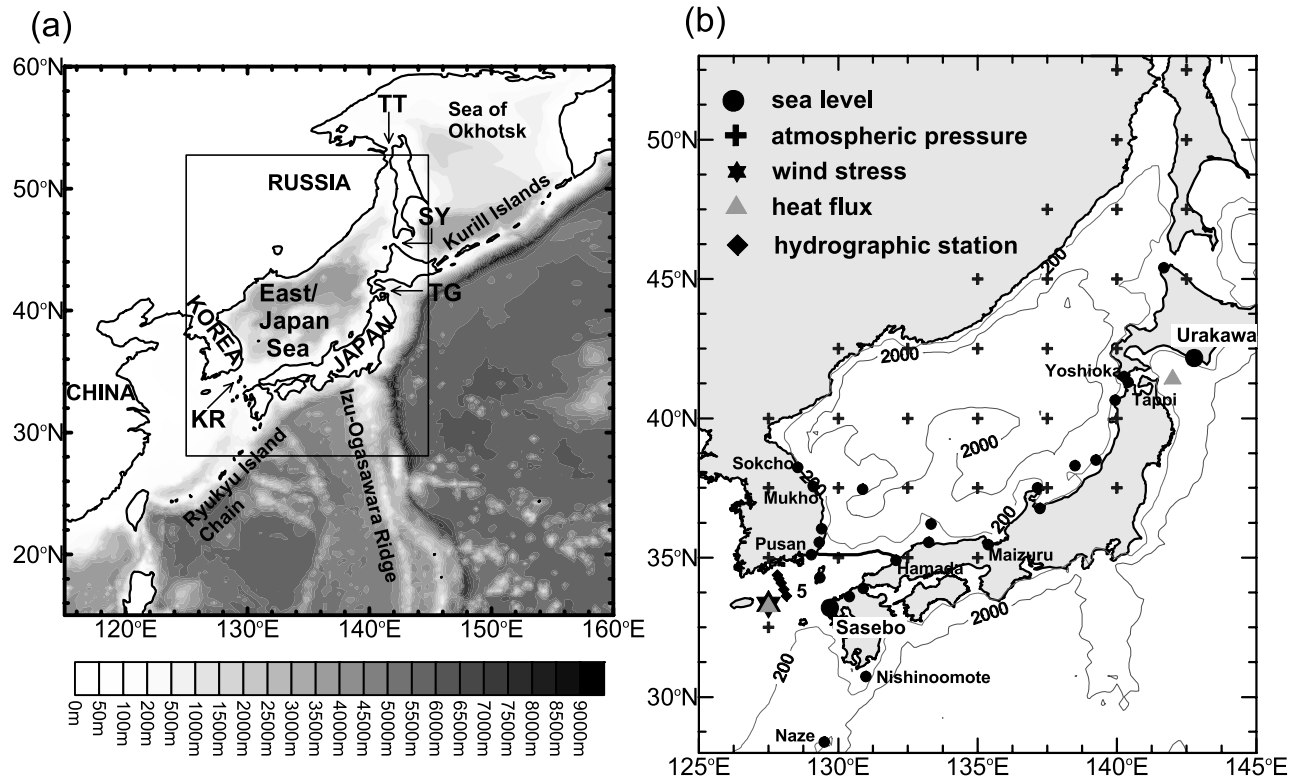

Figure 1. (a) Bottom topography of the East Sea and the northwestern Pacific. Shading contours are depths in meters. KR, TG, SY, and TT denote the Korea, Tsugaru, Soya, and Tartarsky straits, respectively. (b) Station map of sea levels observed at coastal tide gauges, the NCEP/NCAR reanalysis data (atmospheric pressure, wind stress, and surface net heat flux), and hydrographic data of line 205 of KODC. The thick line denotes the submarine cable between Pusan and Hamda.

inflow on a β plane. Both the zonal and meridional SLDs are related to the large-scale wind-driven circulation in the North Pacific [*Nof*, 2000]. However, the wind stress curl over the open ocean is maximum in winter and minimum in fall [*Blaha and Reed*, 1982; *Lee et al.*, 2001], while the transport through the Korea Strait is known to be maximum in summer and fall and minimum in winter and spring [*Teague et al.*, 2002; *Lyu and Kim*, 2003; *Kim et al.*, 2004; *Takikawa et al.*, 2005]. This discrepancy in time may result from topographic blocking of barotropic waves to propagate westward by the Izu-Ogasawara Ridge and the Ryukyu Island chain (Figure 1). These topographic effects were reported in the Kuroshio through the Tokara Strait [*Ichikawa and Beardsley*, 1993; *Kubota et al.*, 1995; *Lee et al.*, 2001; *Isobe and Imawaki*, 2002] as well as in the Florida Current through the Florida Strait [*Lee and Williams*, 1988; *Schott et al.*, 1988].

[4] What drives the flow variations through the straits of the East Sea on short-period subinertial to interannual timescales? *Toba et al.* [1982] proposed that there are seasonal variations in the meridional SLD between the warm area south of the Korea Strait and the cold area east of the Tsugaru Strait and that they are caused mainly by effective air-sea interactions in the shallow East China Sea (Figure 1). However, *Ohshima* [1994] showed that there is a small seasonal change in the meridional geopotential height difference calculated from hydrographic data. Moreover, this steric effect, which results mainly from surface heating and cooling in the midlatitude, is passive, i.e., it does not cause changes in the subsurface pressure and hence does not drive barotropic motion [*Gill and Niiler*, 1973]. *Lee and Williams* [1988] and *Schott et al.* [1988] reported that the local along-strait wind can account for most of the transport variations in the Florida Strait shorter than season and some part of seasonal variations. *Kubota et al.* [1995] and *Lee et al.* [2001] also showed that the seasonal transport variations in the Tokara Strait can be explained by the local along-strait wind.

[5] Recently, *Lyu et al.* [2002] reported that there are nonisostatic subinertial variations with the range of 2–3 Sv on timescales of 3–5 days in the transport through the Korea Strait and that these variations could be derived from the uniform atmospheric pressure over the East Sea acting like a forced oscillator constrained by straits. They showed that these variations are amplified at the period of a Helmholtz resonance between the East Sea and the Pacific Ocean through the straits. These nonisostatic variations were also found in the bottom pressure gauge data in the southwestern part of the East Sea [*Park and Watts*, 2005] and the TOPEX/Poseidon altimeter data over the East Sea [*Nam et al.*, 2004]. However, the driving forces of short-period subinertial to interannual variations in strait flows and the mean sea level of the East Sea have not been clearly understood yet.

[6] This study is aimed at understanding the driving mechanisms of these temporal variations in a barotropic linear system and finding dominant forces on each time-scale. Section 2 describes transport variations from the

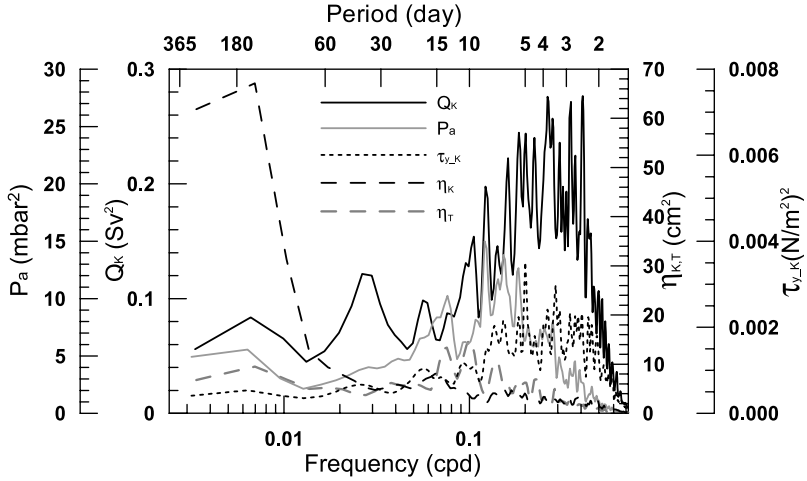

Figure 2. Variance conserved spectra of the transport through the Korea Strait (Q_K), the atmospheric pressure averaged over the East Sea (P_a), the along-strait wind stress at the Korea Strait (τ_{y_K}), and sea levels at Sasebo (η_K) and Urakawa (η_T) (Figure 1) after inverse barometric adjustment.

continuous voltage measurement in the Korea Strait and their relationship with expected forces, such as the atmospheric pressure, the wind stress, and the sea levels outside the straits of the East Sea. In section 3 a simple analytical barotropic model is introduced to investigate the barotropic responses of the East Sea to these forces and then the dominant driving forces are determined on each timescale in section 4. Problems in this model and further interpretations are discussed in section 5 and finally conclusions are given in section 6.

2. Data and Analysis

2.1. Data

[7] The volume transport through the Korea Strait (Q_K) is converted from the motion-induced voltage measured by the submarine cable (Figure 1) from March 1998 to April 2002 using the estimated linear relationship between the voltage and the observed transport [*Kim et al.*, 2004]. The geomagnetic effects on the observed voltage are removed before conversion although they are not significant at periods longer than 2 days.

[8] The NCEP/NCAR reanalysis data of the atmospheric pressure and the wind stress at the surface from January 1998 to April 2002 are obtained from the NOAA-CIRES Climate Diagnostic Center (Figure 1). The data interval is 6 hours and the horizontal grid size is 2.5° × 2.5° for the atmospheric pressure (Figure 1). The atmospheric pressure (P_a) is spatially averaged over the East Sea to obtain representative time series related to the barotropic responses in the East Sea and it accounts for 69% of the total variance. The along-strait wind stress at the Korea Strait (τ_{y_K}) is selected from the NCEP/NCAR reanalysis data at the nearest grid point to the Korea Strait (Figure 1). τ_{y_K} denotes the wind stress in the along-strait direction in the coordinates rotated clockwise by 42.5°.

[9] Korean Oceanographic Data Center (KODC) and Japan Oceanographic Data Center (JODC) provide hourly sea level data at the tidal stations inside and outside the East Sea (Figure 1) for a period of January 1998 to December 2001. The sea levels observed at Sasebo and Urakawa are selected to represent the sea level changes outside the Korea and Tsugaru straits, respectively, which may cause the pressure gradient force at each strait. Conventional inverse barometric adjustment is applied to these two sea level data at Sasebo and Urakawa and we call these adjusted sea levels η_K and η_T, respectively. The mean sea level of the East Sea (η_0) is calculated by spatially averaging the sea levels inside the East Sea (Figure 1) without inverse barometric adjustment and it accounts for 65% of the total variance. The concurrent period of all the data sets is 46 months from March 1998 to December 2001. All the data are low-pass filtered with a cutoff period of 36 hours to investigate subinertial variations only.

2.2. Transport Variations and Their Relationship With Expected Forces

[10] Figure 2 shows variance-conserved spectra of the transport through the Korea Strait (Q_K), the mean atmospheric pressure (P_a), the along-strait wind stress at the Korea Strait (τ_{y_K}), and the adjusted sea levels outside the Korea and Tsugaru straits (η_K, η_T). Q_K has large variance of 0.2∼0.3 Sv^2 at the short periods of 2 to 10 days, which will be called the "subinertial" periods hereinafter. Another variance peak of Q_K occurs on the timescales of 30 to 60 days, which will be called the "monthly" periods. There is a weak semiannual variation in Q_K. Since seasonal to interannual variations cannot be resolved with a statistical significance by spectral analyses due to a data shortage, these long-term variations in Q_K will be analyzed in the time domain.

[11] P_a varies most on the timescales of 3 to 10 days centered at about 7 to 8 days (Figure 2). There is another peak around the period of 14 days, which may be related to the fortnight atmospheric tide. A weak semiannual variation also appears. Most energy in τ_{y_K} is distributed on the subinertial timescales of 2–10 days. The variances of η_K and η_T increase with period at the subinertial periods, maintain approximately constant up to the monthly band, and increase again with period. While η_K has larger variance than η_T at the submonthly periods, η_T has larger variance at the periods of 4–15 days. Some of variations in the adjusted sea levels at low frequen-

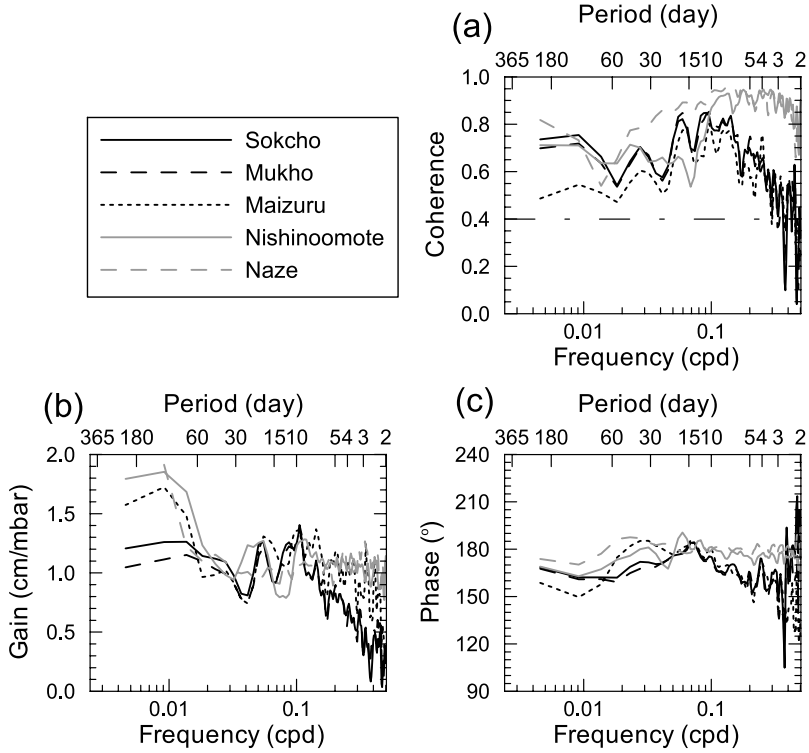

Figure 3. Cross spectra of (a) coherence, (b) gain, and (c) phase between atmospheric pressure and sea levels at Sokcho, Mukho, Maizuru, Nishinoomote, and Naze (Figure 1). Atmospheric pressure data are selected nearest to each tidal station from NCEP reanalysis data. The dash-dotted line in Figure 3a indicates the 95% confidence level [*Emery and Thomson*, 1998].

cies may be caused by the steric effects, which will be estimated in the next section and removed from the adjusted sea levels.

[12] Inverse barometric response of the sea level to the atmospheric pressure is investigated outside as well as inside the East Sea by using the sea level at each tidal station without inverse barometric adjustment and the atmospheric surface pressure from NCEP reanalysis data nearest to each tidal station (Figure 1). The coherences between the atmospheric pressures and the sea levels measured at Sokcho, Mukho, and Maizuru inside the East Sea are higher than 0.5 at the periods longer than 4 days (Figure 3a). Their coherences decrease and often become lower than the 95% confidence level at the periods of 2 to 4 days. The sea level response to the atmospheric pressure inside the East Sea deviates from the isostatic response as expected in the open ocean. That is, their gain decreases with frequency from 1 cm/mbar to about 0.3 cm/mbar and their phase difference changes from 180° to 130° in this subinertial band (Figures 3b and 3c). The response of the local sea level, however, becomes isostatic again at the periods shorter than 2 days (not shown here). On the timescales of 10 to 60 days their gain varies around 1 cm/mbar and their phase difference remains about 180°. On the other hand, sea levels measured at Nishinoomote and Naze outside the East Sea are highly correlated with the atmospheric pressure, especially at the subinertial periods (Figure 3a). The gains are nearly 1 cm/mbar at the periods of 2–60 days and the phase differences are close to 180° on the whole timescales (Figures 3b and 3c). Note that the gains at Maizuru, Nishinoomote, and Naze have values larger than 1.5 cm/mbar at the periods longer than 90 days, which may be related to other factors such as the local wind stress [*Kubota et al.*, 1995] and the baroclinic Rossby waves propagated from the east [*Isobe and Imawaki*, 2002].

[13] Since the atmospheric pressure is strongly correlated with wind stresses and sea levels measured at coastal tide gauges may be affected by both of them, multiple coherence analyses are conducted to find relationships between Q_K and its four expected driving forces (P_a, τ_{y_K}, η_K, and η_T) (Figures 4a and 4b). In Figure 4 (also in Figure 5) the degree of freedom for the subinertial periods of 2–10 days is increased 3 times larger than that for the periods longer than 10 days to increase visibility at the subinertial periods. The squared multiple coherence of Q_K with four inputs (P_a, τ_{y_K}, η_K, and η_T) has high values of 0.5–0.9 over the whole period. Comparison of Q_K with the spatially averaged atmospheric pressure (P_a) reveals that their squared partial coherence is very high at the subinertal period and generally decreases with period. Their gain has a peak of 0.10–0.15 Sv/mbar and Q_K leads P_a by 120°–240° (solid dots in Figures 5a and 5b) on the timescales of 2–4 days. If the sea level can respond isostatically to the atmospheric pressure in the East Sea, Q_K should lead P_a by 270° by continuity. Figure 5b also shows that there is a nonisostatic response in the East Sea at the subinertial periods.

[14] While Q_K has a lower squared partial coherence with the along-strait wind stress at the Korea Strait (τ_{y_K}) at the subinertial periods than that with P_a, Q_K is more highly correlated with τ_{y_K} at the monthly periods (Figure 4a). Their gain is about 5–9 Sv/N/m^2 and their phase difference is near 0

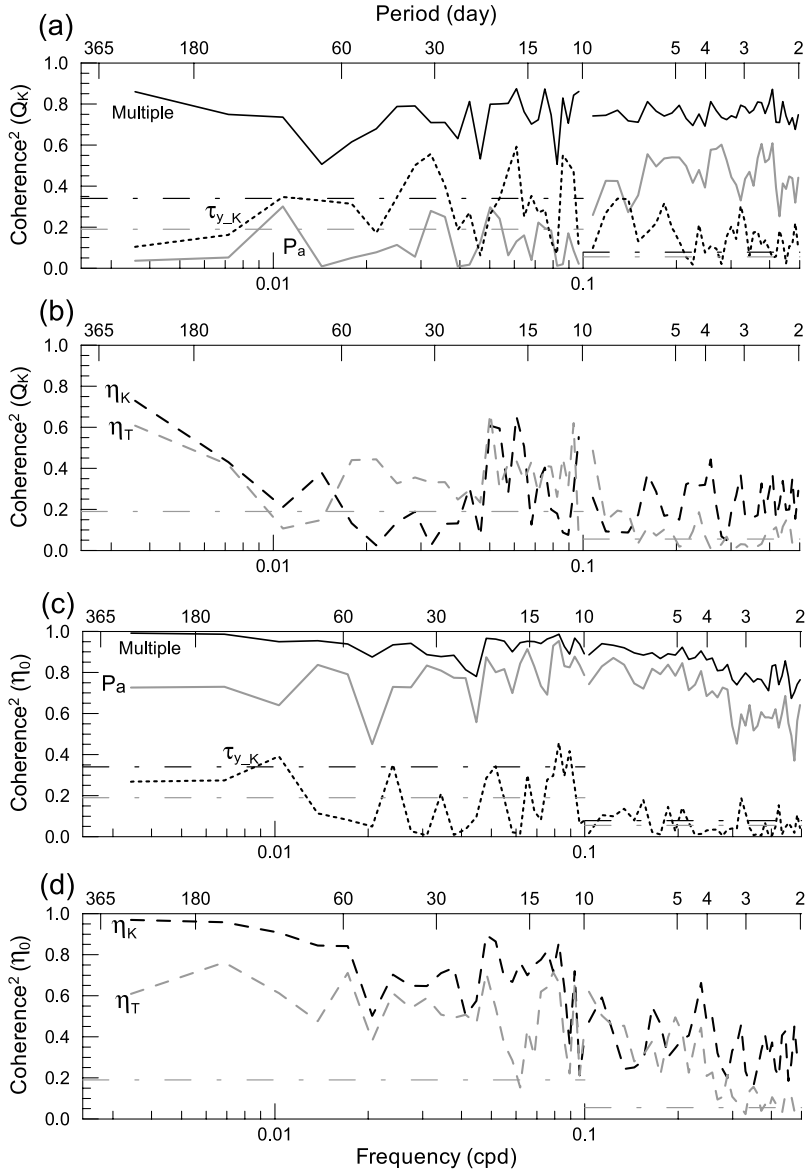

Figure 4. Multiple and partial squared coherences (a, b) between Q_K and four inputs (P_a, τ_{y_K}, η_K, and η_T) or (c, d) between η_0 and four inputs. Dash-dotted and shaded dash-dotted lines indicate the 95% confidence levels for multiple and partial coherences [*Otnes and Enochson*, 1972], respectively.

at the monthly periods (solid dots in Figures 5c and 5d). Q_K seems to lag behind τ_{y_K} at the periods shorter than 4 days. Q_K also has a high coherence with the adjusted sea level changes at Sasebo (η_K) in the subinertial and very low frequency bands (Figure 4b). Their gain has a peak of about 0.1 Sv/cm at the subinertial periods and decreases with period converging to about 0.05 Sv/cm at longer periods (solid dots in Figure 5e). They are approximately in phase at all periods except the subinertial periods (solid dots in Figure 5f). The adjusted sea level changes at Urakawa (η_T) are significantly correlated with Q_K at the monthly and longer periods (Figure 4b), where they are out of phase and their gains are about 0.05–0.8 Sv/cm (solid dots in Figures 5g and 5h).

[15] The mean sea level of the East Sea (η_0), which is calculated by spatially averaging the sea levels inside the East Sea, is also compared with four inputs through multiple coherence analyses. Their squared multiple coherence is almost 0.8 or higher over the whole period (Figure 4c). The squared partial coherence of η_0 with P_a is also very high in all the period bands (Figure 4c). Their gain has values around 1 cm/mbar at long periods but it tends to decrease with wide ranges at the subinertial periods (shaded dots in Figure 5a). While their phase difference is about 180° at the periods longer than 10 days, it decreases to 90° at the subinertial periods (shaded dots in Figure 5b). These results also show the nonisostatic response in the East Sea at the subinertial periods. η_0 has low squared partial coherences with τ_{y_K} (Figure 4c). Their gain increases from 10 cm/N/m^2 to 30 cm/N/m^2 with period and they are in phase at long periods but η_0 lags behind τ_{y_K} at the subinertial periods (shaded dots in Figures 5c and 5d). On the contrary, η_0 has high coherences with η_K and η_T especially at long periods (Figure 4d). η_0 and η_K are approximately in phase at the monthly and longer periods with their gain of about 0.5–

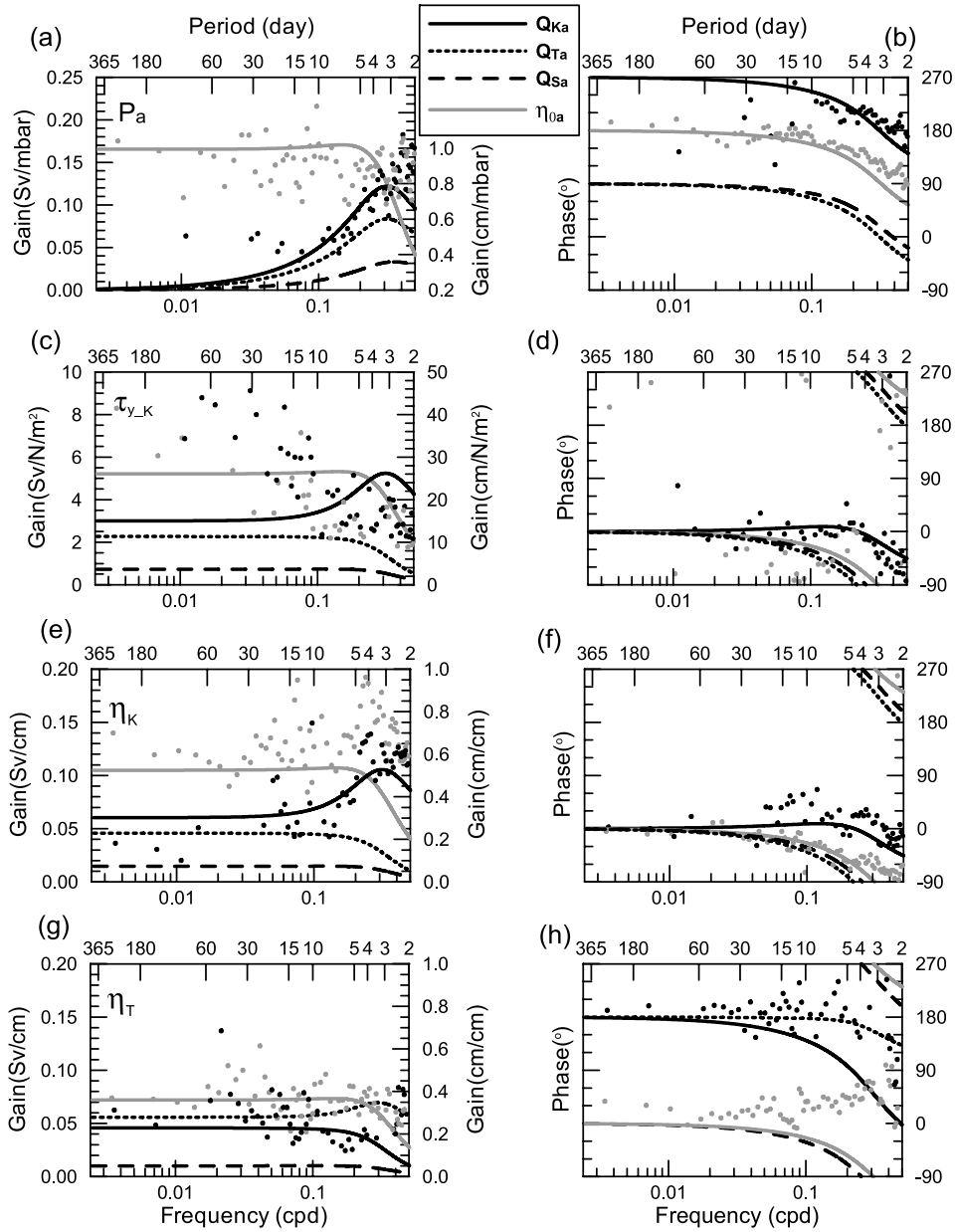

Figure 5. Analytically obtained gain and phase relations of Q_K (solid line), Q_T (dotted line), Q_S (dashed line), and η_0 (shaded line) with (a, b) P_a, (c, d) τ_{y_K}, (e, f) η_K, and (g, h) η_T. Solid and shaded dots denote relations of the observed Q_K and η_0 with observed P_a, τ_{y_K}, η_K, and η_T, which are calculated from the multiple coherence analysis as in Figure 4.

0.7 cm/cm and their phase decreases about to $-90°$ at the subinertial periods (shaded dots in Figures 5e and 5f). The gain between η_0 and η_T is 0.3–0.5 cm/cm and their phase is about 0° at the monthly and longer periods (shaded dots in Figures 5g and 5h).

[16] Since most variations in Q_K and atmospheric forces occur at the subinertial, monthly, and longer periods (Figure 2) and the steric height anomaly can be assumed to vary on the timescales longer than the semiannual period, all the data are split into two time series: one is band-pass filtered for the periods of 2–60 days to analyze subinertial to monthly variations, and the other is low-pass filtered with a cutoff period of 90 days to analyze seasonal to interannual variations. Steric effects on sea levels measured at tidal gauges will be considered only on the seasonal to interannual timescales.

3. An Analytical Model

[17] As shown in the previous section, the transport in the Korea Strait (Q_K) and the mean sea level of the East Sea (η_0) are highly correlated with the atmospheric pressure, the along-strait wind stress, and the adjusted sea level changes outside the straits of the East Sea. To investigate the barotropic response of the East Sea to these forces, a simple analytical model is introduced. In this model the East Sea is considered as a deep flat-bottomed basin connected to the open ocean through only three straits (Figure 6) because the

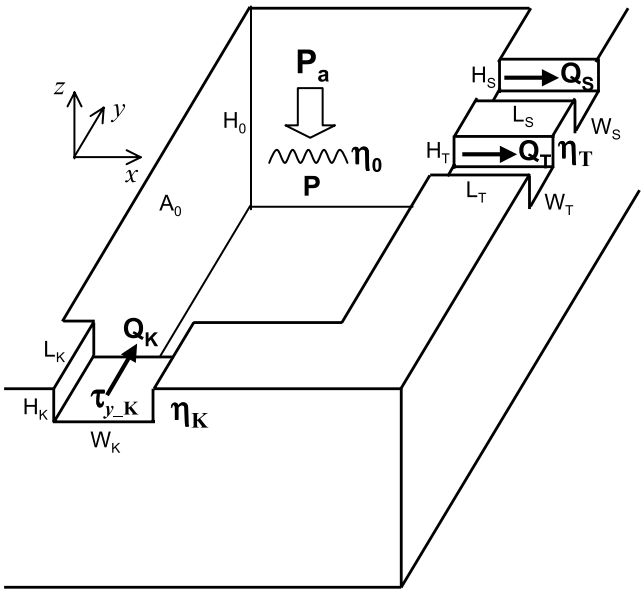

Figure 6. Schematic diagram of a simple model. Subscripts K, T, and S designate the Korea, Tsugaru, and Soya straits, respectively. Q, L, W, and H are the volume transport, the along-strait length, the width, and the depth of each strait, respectively. P_a is the uniform atmospheric pressure over the East Sea. P, η_0, A_0, and H_0 are the subsurface pressure, the mean sea level, the surface area, and the depth of the East Sea, respectively; η_K and η_T designate the adjusted sea levels outside the Korea and Tsugaru straits, respectively, and τ_{y_K} denotes the along-strait wind stress at the Korea Strait.

transport through the Tatarsky Strait (Figure 1) is negligible. The water density is homogeneous and the depth in the basin is constant as the mean depth of the East Sea: H_0 = 1700 m. The depth (H), the width (W), and the along-strait length (L) of each strait are estimated roughly as shown in Table 1. Since the East Sea is deep and its horizontal length scale is about 1000 km, long gravity waves travel so fast within the basin that the mean sea level (η_0) and the subsurface pressure (P) of the East Sea can be considered spatially uniform on the timescales longer than the inertial period [*Lyu et al.*, 2002]. Since the system is linear and the expected forces are assumed independent of each other, each force will be separately dealt with in the following subsections.

3.1. Atmospheric Pressure

[18] *Garrett and Majaess* [1984] found nonisostatic responses of the sea level to the atmospheric pressure in the eastern Mediterranean. *Candela et al.* [1989] also reported nonisostatic subinertial variations in the transport through the Strait of Gibraltar and the sea level in the Mediterranean Sea. They explained those nonisostatic variations by a Helmholtz resonance of the Mediterranean with the Atlantic through the Strait of Gibraltar. Recently, a Helmholtz resonance was also reported in the East Sea [*Lyu et al.*, 2002; *Nam et al.*, 2004; *Park and Watts*, 2005] because it is also a semienclosed marginal sea communicating with the Pacific through shallow straits.

[19] We describe below the main aspects of the nonisostatic response of the East Sea to the atmospheric pressure based on *Lyu et al.* [2002]. The cross-strait geostrophic balance is well justified at the three straits by scale analysis as verified for the Korea Strait by *Mizuno et al.* [1989]. The flows through the straits may be restricted by the bottom friction and the "geostrophic control" [*Toulany and Garrett*, 1984]. The bottom friction is linearly parameterized as $\lambda_f Q$ ($\lambda_f = C_0 U/H$) [*Candela et al.*, 1989], where Q is the volume transport through each strait, C_0 a drag coefficient (3×10^{-3}), and U a characteristic along-strait current speed. The geostrophic control is estimated as $\lambda_g Q$ ($\lambda_g = fW/2L$) [*Wright*, 1987], where f is the Coriolis parameter (0.9×10^{-4} s^{-1}). If we consider a linearly combined term of the bottom friction and the geostrophic control and the cross-strait current speed is assumed one order of magnitude less than U, the advection and the Coriolis term in the along-strait momentum equation are one order magnitude less than the friction term at the three straits. The momentum equations in the along-strait direction are given as follows after integrating in the vertical section across the strait (Figure 6).

$$\frac{\partial Q_K}{\partial t} = -\frac{A_K}{\rho}\frac{\partial P}{\partial y} - \lambda_K Q_K \tag{1a}$$

$$\frac{\partial Q_T}{\partial t} = -\frac{A_T}{\rho}\frac{\partial P}{\partial x} - \lambda_T Q_T \tag{1b}$$

$$\frac{\partial Q_S}{\partial t} = -\frac{A_S}{\rho}\frac{\partial P}{\partial x} - \lambda_S Q_S, \tag{1c}$$

where A is the vertical cross-sectional area of each strait, P the subsurface pressure, and ρ a constant water density: ρ = 1027 kg m^{-3}. The subscripts, K, T, and S, designate the Korea, Tsugaru, and Soya straits, respectively. The positive direction of the volume transport at each strait is defined in the positive x or y direction in Figure 6: Positive Q_K means the flow into the East Sea, while Q_T and Q_S mean the flows out of the basin. The continuity is given as

$$A_0 \frac{\partial \eta_0}{\partial t} = Q_K - Q_T - Q_S, \tag{2}$$

Table 1. Characteristic Scales and the Estimated Combined Linear Friction Coefficient (λ) at the Three Straits of the East Sea[a]

Strait	U, m/s	W, 10^5 m	H, m	A, 10^6 m^2	L, 10^5 m	λ, 10^{-5}s^{-1}	FG
Korea	0.2	1.7	80	13.6	4	2.7	0.4
Tsugaru	0.7	0.2	120	2.4	1	2.7	1.9
Soya	0.5	0.4	40	1.6	1	5.6	2.1

[a]FG is the ratio of the bottom friction ($\lambda_f = C_0 U/H$) to the geostrophic control ($\lambda_g = fW/2L$) at each strait (FG = $\lambda_f/\lambda_g = 2L\lambda_f/fW$), where C_0 is the drag coefficient and f is the Coriolis parameter. U is the characteristic along-strait current speed, and A is the cross-sectional area of each strait. All other notations are defined in Figure 6.

where A_0 is the surface area of the East Sea: $A_0 = 1.3 \times 10^{12}$ m^2. The subsurface pressure (P) is composed of the atmospheric pressure (P_a) and the hydrostatic contribution of the sea surface elevation (η_0):

$$P = P_a + \rho g \eta_0, \tag{3}$$

where g is the acceleration due to gravity: $g = 9.8$ m s^{-2}. It is assumed that the sea surface in the open ocean responds isostatically to the atmospheric pressure forcing. Since it is the pressure difference through the strait that drives the motion, P outside the basin can be taken to be zero for convenience.

[20] Since the system is linear and there are five equations with five unknowns, taking all of them to behave as $\exp(i\omega t)$ and approximating the pressure gradient such as $\partial P/\partial y \sim (P_a + \rho g \eta_0)/L_K$, we can solve the problems to get, for example, the solution of Q_K with P_a as a force.

$$Q_K = \frac{i\omega}{D} b_K \{-\omega^2 + \lambda_T\lambda_S + i(\lambda_T + \lambda_S)\omega\} P_a, \tag{4}$$

$$\begin{aligned} D = D_0 &+ (\lambda_K\lambda_T + \lambda_T\lambda_S + \lambda_S\lambda_K)\omega^2 \\ &- (\lambda_K\lambda_T c_S + \lambda_T\lambda_S c_K + \lambda_S\lambda_K c_T) \\ &+ i\omega[(\lambda_K + \lambda_T + \lambda_S)\omega^2 - \{(c_T + c_S)\lambda_K \\ &+ (c_S + c_K)\lambda_T + (c_K + c_T)\lambda_S + \lambda_K\lambda_T\lambda_S\}] \end{aligned} \tag{5}$$

$$D_0 = -\omega^2\{\omega^2 - (c_K + c_T + c_S)\}, \tag{6}$$

where $b_K = \frac{A_K}{\rho L_K}$ and $c_{K,T,S} = \frac{gA_{K,T,S}}{A_0 L_{K,T,S}}$.

[21] There is a Helmholtz resonance between the East Sea and the Pacific Ocean through the three straits, the frequency (ω_0) of which is given by the root of (6). This period is related to the timescale for the basin to be filled or drained by the strait flows and is estimated at about 3 days for the East Sea using the values listed in Table 1, which is related to the periods of nonisostatic subinertial variations shown in Figures 3, 5a, and 5b.

[22] The amplitude ratios (gains) and the phase relations between the atmospheric pressure and the transport at each strait ($Q_{K,T,S}$) or the mean sea level of the East Sea (η_0) are analytically estimated (Figures 5a and 5b) by assuming $\lambda_K = 2.7 \times 10^{-5}$ s^{-1}, $\lambda_T = 2.7 \times 10^{-5}$ s^{-1}, and $\lambda_S = 5.6 \times 10^{-5}$ s^{-1}, which are obtained from estimated characteristic length scales and mean current speeds at each strait (Table 1). At the subinertial periods the gain from P_a to Q_K has a peak of 0.12 Sv/mbar near a Helmholtz resonant period of about 3 days and their phase varies from 270° to 150° at these periods. When the relevant timescale gets longer, the isostatic response is restored: P_a leads Q_K by 90° and the gain from P_a to Q_K decreases sharply due to the low frequencies. The isostatic response remains between P_a and η_0 with gain of 1 cm/mbar and phase of 180° at the periods longer than 10 days. On the other hand, their relations show nonisostatic responses at the subinertial periods: Their gain decreases from 1.0 to 0.4 cm/mbar and their phase difference changes from 180° to 60°. Considering the simplicity of the model, the observed gain and phase relations between P_a and Q_K or η_0 (solid and shaded dots in Figures 5a and 5b) are reasonably reproduced. The gains from P_a to Q_T and Q_S have also peaks at the 3-day period but their values are smaller than that from P_a to Q_K. Their phase relations are out of phase with that between Q_K and P_a over the whole period: When P_a increases, the water flows out of the basin through the three straits and η_0 drops down by continuity, and vice versa.

3.2. Wind Stress

[23] *Csanady* [1982] demonstrated that the unidirectional wind effect is negligible in an enclosed basin when its horizontal scale is smaller than the external Rossby radius of deformation, which is about 1300 km in the East Sea. However, the flow through a shallow strait can be driven by the local along-strait wind stress, geostrophically balancing with the pressure gradient force across the strait [*Hannah*, 1992; *Middleton and Viera*, 1991].

[24] The momentum equation in the along-strait direction at the Korea Strait, for example, is given as

$$\frac{\partial Q_K}{\partial t} = -\frac{A_K}{\rho}\frac{\partial P}{\partial y} + \frac{A_K}{\rho H_K}\tau_{y\_K} - \lambda_K Q_K, \tag{7}$$

where τ_{y_K} is the along-strait wind stress at the Korea Strait (Figure 6). If the strait connects two semi-infinite basins, there is no wind-driven pressure gradient between two basins as in the case of the Bass Strait southeast of Australia [*Hannah*, 1992]. Since we consider a finite basin connected to the open ocean through straits, the subsurface pressure (P) only inside the basin may be changed with the mean sea level of the basin (η_0) as $P = \rho g \eta_0$ and η_0 is related to the net transport through the three straits by continuity (2). The momentum equations at the Tsugaru and Soya straits can be written in the same way as (7) with each along-strait wind stress (τ_{x_T}, τ_{x_S}).

[25] These linear equations will give, for example, the solution of Q_K with τ_{y_K}, τ_{x_T}, and τ_{x_S} as given forces.

$$\begin{aligned} Q_K = &\frac{i\omega}{D}[\{\omega^2 - (c_T + c_S + \lambda_T\lambda_S)\}a_K\tau_{y\_K} - a_T c_K \tau_{x\_T} - a_S c_K \tau_{x\_S}] \\ &+ \frac{1}{D}[\{(\lambda_T + \lambda_S)\omega^2 - (c_T\lambda_S + c_S\lambda_T)\}a_K\tau_{y\_K} \\ &- a_T c_K \lambda_S \tau_{x\_T} - a_S c_K \lambda_T \tau_{x\_S}], \end{aligned} \tag{8}$$

where $a_{K,T,S} = \frac{A_{K,T,S}}{\rho H_{K,T,S}}$.

[26] Using the values of the frictional coefficients in Table 1, the amplitude and phase relations between τ_{y_K} and $Q_{K,\ T,\ S}$ or η_0 are given as in Figures 5c and 5d. The observed cross spectra, gain and phase, between τ_{y_K} and Q_K or η_0 (solid and shaded dots in Figures 5c and 5d) are also compared to the analytically obtained cross spectra. Phase relationships are relatively well reproduced over the whole period but the gains are not so well especially for Q_K at the monthly periods. The gain between Q_K and τ_{y_K} has a peak of about 5.2 Sv/N/m^2 at the 3-day period, which is also related to the Helmholtz resonance similar to the case of P_a. Q_K (η_0) lags τ_{y_K} by 45° (135°) at the 2-day period. On the other hand, the gain between Q_T or Q_S and τ_{y_K} has no peak and Q_T and Q_S lags behind Q_K by about 90° at short periods. The sum of gains of Q_T and Q_S is smaller than the gain of Q_K at the periods shorter than about 15 days and it becomes the same at longer periods. The gain of η_0 increases with period up to the 5-day period, decreases slightly and then

has a constant value of 26 cm/N/m^2 at long periods. The gains from τ_{y_K} to $Q_{K,T,S}$ converge to constant values of about 3, 2.3, and 0.7 Sv/N/m^2 at low frequencies and they are all in phase.

[27] From these gain and phase relationships we can infer how the wind stress drives the strait flows and changes the mean sea level in the East Sea. If τ_{y_K} starts, for example, to act in the positive y direction over the Korea Strait (Figure 6) from a static state, the wind-forced inflow, Q_K, will be driven and the sea level inside the basin (η_0) will increase because all the inflow, Q_K, cannot simultaneously flow out of the basin through the Tsugaru and Soya straits due to the finite volume of the straits and the friction in the straits. While Q_K increases with time by τ_{y_K}, the friction also gets stronger with Q_K and the increased η_0 causes the pressure gradient force in the negative y direction at the Korea Strait and in the positive x direction at the Tsugaru and Soya straits to induce outflows ($Q_{T,S}$) from the East Sea. At the low frequencies there is enough time that the wind-forced flow through the Korea Strait can go out of the basin through other two straits and there is not an additional change in η_0. A steady state will be reached in the Korea Strait by balancing among the three forcing terms: wind stress, pressure gradient force, and friction. On the other hand, the pressure gradient force caused by τ_{y_K} is balanced with the friction at the Tsugaru and Soya straits at low frequencies.

[28] The wind stresses at the Tsugaru and Soya straits (τ_{x_T}, τ_{x_S}) drive the strait flows and change η_0 in the same manner as τ_{y_K}. However, their gains are quite small compared with that of τ_{y_K} (not shown here). This is caused mainly by the fact that the magnitude of wind-forced flow is proportional to the width of the strait and inversely proportional to the friction as in (7). If we use the widths and frictions of the Tsugaru and Soya straits as in Table 1, their wind stress effects are estimated one order of magnitude smaller than that of the Korea Strait. We therefore will consider only the effect of the wind stress at the Korea Strait (τ_{y_K}) in this study.

3.3. Sea Level Changes Outside the Straits of the East Sea

[29] Many researches have been done on subinertial flows driven by the SLD between the opposite ends of the strait connecting two basins [*Toulany and Garrett*, 1984; *Wright*, 1987]. In this study we do not try to find what drives the variations in the adjusted sea levels outside the straits of the East Sea but just use these adjusted sea level variations as forces to induce flows through the straits of the East Sea.

[30] Suppose that there is a sea level difference ($\eta_K - \eta_0$) along the Korea Strait (Figure 6). Since the Kelvin wave is trapped against its wall southwest of the Korea Strait, the adjusted sea level at the southeast corner of the strait (η_K) remains close to the interior value of the open ocean. On the other hand, the sea level inside the basin can be assumed homogeneous as η_0 at the subinertial periods. The along-strait momentum equation for the Korea Strait is given as

$$\frac{\partial Q_K}{\partial t} = \frac{gA_K}{L_K}(\eta_K - \eta_0) - \lambda_K Q_K. \tag{9}$$

The along-strait momentum equations for the Tsugaru and Soya straits can be represented in the same way with the adjusted sea levels (η_T, η_S) outside the straits as forces. Furthermore, it is assumed that the Kelvin waves propagating from the Tsugaru and Soya straits along the outside of the East Sea do not perturb the sea levels near the Korea and Tsugaru straits, respectively, because the barotropic Kelvin waves may be blocked by topography such as the Izu-Ogasawara Ridge and the Kuril Islands (Figure 1). That is, the adjusted sea levels outside the straits do not affect each other and hence can be considered as independent forces.

[31] Since we have four unknowns (Q_K, Q_T, Q_S, η_0) and four linear equations including the continuity (2), the solution of Q_K, for example, with the adjusted sea levels outside the straits as forces is given as

$$\begin{aligned} Q_K = {} & \frac{i\omega}{D}\left[\left\{\omega^2 - (c_T + c_S + \lambda_T\lambda_S)\right\}c_K\eta_K + c_Tc_K\eta_T + c_Sc_K\eta_S\right] \\ & + \frac{1}{D}\left[\left\{(\lambda_T + \lambda_S)\omega^2 - (c_T\lambda_S + c_S\lambda_T)\right\}c_K\eta_K \right. \\ & \left. + c_Tc_K\lambda_S\eta_T + c_Sc_K\lambda_T\eta_S\right]. \end{aligned} \tag{10}$$

[32] The amplitude and phase relations between the adjusted sea levels (η_K, η_T) and $Q_{K,\ T,\ S}$ or η_0 are calculated by using the frictional coefficients in Table 1 (Figures 5e, 5f, 5g, and 5h). These relations are very similar to those between τ_{y_K} and $Q_{K,\ T,\ S}$ or η_0 except that the effect of η_T is not so small compared with that of η_K. This result originates mainly from the fact that if the flow is geostrophically balanced, its volume transport depends on the depth of the strait for a given sea level difference. The driving mechanism of the pressure-forced flows through the straits and the mean sea level variations in the East Sea can be interpreted in the same way as the wind-forced flows in section 3.2. At long periods the gains from η_K to $Q_{K,T,S}$ and η_0 converge to constant values of about 0.060, 0.045, 0.015 Sv/cm, and 0.52 cm/cm, respectively and they are all in phase (Figures 5e and 5f). The gains from η_T to Q_K and η_0 converge also to constant values smaller than those from η_K to Q_K and η_0 at long periods (Figure 5g). η_T is out of phase with Q_K and Q_T and it is in phase with Q_S and η_0 at long periods (Figure 5h). The observed gain and phase relations (solid and shaded dots in Figures 5e, 5f, 5g, and 5h) are roughly reproduced for η_K and η_T by this simple analytical model except for η_T at the subinertial periods. Note that the partial coherence between η_T and Q_K or η_0 is relatively low and noisy at the subinertial periods (shaded dashed lines in Figures 4b and 4d).

[33] Since Sasebo and Urakawa are located at the places outside the Korea and Tsugaru straits where the Kelvin waves do not propagate (Figure 1), they can be considered as proper representatives (η_K and η_T) of the interior values outside the straits. There are, however, no available tide gauge data at the northeastern corner of the Soya Strait. Nonetheless, neglecting the role of η_S in explaining the variations of Q_K and η_0 may not be crucial because the analytically obtained gain from η_S to Q_K or η_0 (not shown here) is smaller than that from η_K to Q_K or η_0 by factor of 4 or 8.

4. Dominant Forces on Each Timescale

[34] In the previous section a simple analytical model was introduced to investigate linear barotropic responses of the

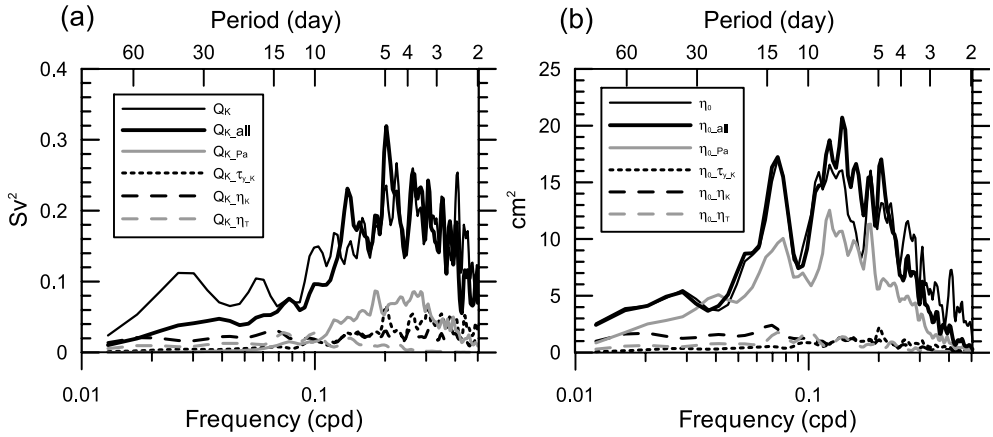

Figure 7. (a) Variance conserved spectra of the voltage-derived transport in the Korea Strait (Q_K) and analytically reproduced transports from each force ($Q_{K\_}P_a$, $Q_{K\_}\tau_{y\_K}$, $Q_{K\_}\eta_K$, $Q_{K\_}\eta_T$) on the subinertial to monthly timescales. (b) Same as Figure 7a except for the mean sea level of the East Sea (η_0) and the analytically reproduced mean sea level. Q_{K_all} and η_{0_all} denote the sums of all the effects.

East Sea to the various forces: the atmospheric pressure (P_a), the along-strait wind stress at the Korea Strait (τ_{y_K}), and the adjusted sea levels (η_K, η_T) outside the East Sea. In this section the effects of each force on variations in transports ($Q_{K,T,S}$) and the mean sea level (η_0) of the East Sea are quantified and then dominant forces are determined on each timescale.

[35] The time series of $Q_{K,T,S}$ and η_0 can be analytically reproduced as follows. First, Fourier transforms are applied to the observed time series of P_a, τ_{y_K}, η_K, and η_T and then they are multiplied by cross spectra, gain and phase, which are analytically obtained as in Figure 5. Finally, analytically reproduced time series of $Q_{K,T,S}$ and η_0 are acquired by inverse Fourier transformations. Since the system is linear, each reproduced time series can be simply added to get the sum (Q_{K,T,S_all}, η_{0_all}) of all the effects, which will be compared to the observed $Q_{K,T}$ and η_0.

4.1. Subinertial to Monthly Variations

[36] Figure 7a shows overall variance distributions of each analytically reproduced transport through the Korea Strait and the observed (voltage-derived) transport (Q_K) in the frequency domain. At the subinertial periods of 2–10 days the atmospheric pressure (P_a) is the most dominant force to drive changes in Q_K due to the Helmholtz resonance as $Q_{K\_}P_a$ in Figure 7a. $Q_{K\_}P_a$ decreases rapidly with period because there is enough time for the East Sea to be drained or filled through the strait flows as it responds isostatically to P_a. The along-strait wind stress at the Korea Strait (τ_{y_K}) causes the wind-driven flow $Q_{K\_}\tau_{y\_K}$, which is comparable to $Q_{K\_}P_a$ at the periods of 2–3 days. However, the variance of $Q_{K\_}\tau_{y\_K}$ decreases with period mainly because most variations in τ_{y_K} are concentrated at the subinertial periods as shown in Figure 2. The changes in the adjusted sea level south of the Korea Strait (η_K) induce the pressure-driven flow $Q_{K\_}\eta_K$, whose variance is comparable to that of $Q_{K\_}P_a$ at the periods of 2–3 days and larger than any other effects at the periods longer than 10 days. On the other hand, the effect of η_T on Q_K is negligible in the subinertial band and increases with period to play the second important role in the total variations of Q_K at longer periods. The sum of all the effects (Q_{K_all}) has comparable variance to that of the observed Q_K at the subinertial periods but it is underestimated as half of the observed variance at the monthly periods. The coherence between Q_K and Q_{K_all} is 0.8–0.9 and their phase difference is close to 0° over the whole period (not shown here). These results imply that most of subinertial to monthly variations in Q_K can be explained by barotropic responses of the East Sea to the forces such as P_a, τ_{y_K}, η_K, and η_T.

[37] The time series of Q_{K_all} show a close agreement to those of Q_K in terms of magnitude and phase with their correlation coefficient of 0.75 (Figure 8b). They show large variations of 1–3 Sv within 3–5 days and they are prevailing especially in winter and spring when P_a changes with a large range on the short-period subinertial timescale. Since there are no available observations of Q_T and Q_S, the sea level difference (SLD) across the Tsugaru Strait between Tappi and Yoshioka (Figure 1) is compared with the analytically reproduced transport Q_{T_all} (Figure 8c). Unfortunately there are no available sea level data at the northern part of the Soya Strait. The SLD across the Tsugaru Strait is scaled for comparison with Q_{T_all} on the assumption of the barotropic and geostrophic flow through the Tsugaru Strait. That is, SLD of 10 cm corresponds to transport of 1.3 Sv if the mean depth of the Tsugaru Strait is 120 m (Table 1). The SLD across the Tsugaru Strait and Q_{T_all} show roughly similar time series in terms of magnitude and phase. Subinertial variations in Q_{T_all} have ranges of 1–2 Sv and they are approximately out of phase with those in Q_{K_all} and in phase with those in Q_{S_all} (Figures 8b, 8c, and 8d). These phase relations result from the subsurface pressure difference between the East Sea and the open ocean, which is caused mainly by nonisostatic response of the East Sea to the atmospheric pressure changes at the subinertial periods. However, monthly variations in Q_{K_all} and Q_{T_all} have ranges of about 1 Sv and they are nearly in phase (Figures 8b and 8c). Subinertial and monthly variations in Q_{S_all} are very weak (Figure 8d) due to a small vertical section of the Soya Strait as shown in the analytically obtained gains from each force to Q_S (Figure 5).

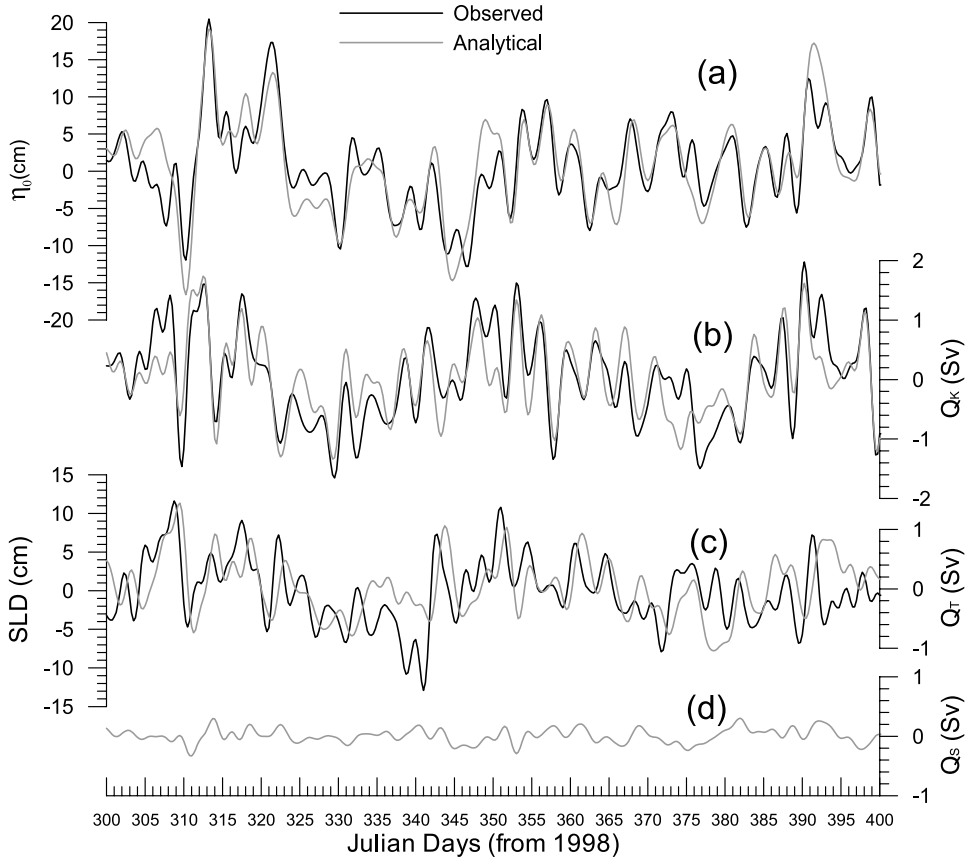

Figure 8. Observed (solid line) and analytically reproduced (shaded line) time series of (a) the mean sea level of the East Sea and transports at the (b) Korea, (c) Tsugaru, and (d) Soya straits on the subinertial to monthly timescales. Shaded lines denote the sum of all time series analytically reproduced by each force. Transport through the Tsugaru Strait is compared with the sea level difference (SLD) between Tappi and Yoshioka (Figure 1), where the SLD is scaled for comparison with Q_{T_all} on the assumption of the barotropic and geostrophic flow through the Tsugaru Strait.

[38] Figure 7b demonstrates the variance distributions of each analytically reproduced mean sea level in the East Sea and the observed mean sea level (η_0). Most variations in η_0 at the subinertial to monthly periods can be explained by barotropic responses of the East Sea to P_a ($\eta_0\_P_a$ in Figure 7b). Contrary to Q_K, the effects of P_a on η_0 do not decrease with period because the sea level inside the East Sea adjusts isostatically to changes in P_a at low frequencies. Since the adjusted sea level changes outside the straits ($\eta_{K,T}$) induce the pressure-driven transport and this volume transport does not flow out instantaneously through other straits, η_0 changes by continuity. η_K plays a significant role in variations of η_0 at the monthly and longer periods. The sum of all the effects (η_{0_all}) has comparable variances with that of η_0 at the subinertial to monthly periods. The coherence between η_0 and η_{0_all} is 0.7–0.9 at the subinertial to monthly periods and they are almost in phase (not shown here). η_{0_all} has very similar time series to those of η_0 in terms of magnitude and phase with their correlation coefficient of 0.88 (Figure 8a). They show clear subinertial variations with a range of 10–30 cm.

4.2. Seasonal to Interannual Variations

[39] On the timescales longer than the semiannual period, sea levels measured at surface tide gauges may include significant passive steric effects, which result mainly from surface heating and cooling over a large area. The steric sea level anomaly (η_α) is estimated in the upper surface layer of 200 m according to the method suggested by *Stammer* [1997]. It is assumed that the effect of changes in salinity on the steric height anomaly is negligible based on the previous estimates of *Gill and Niiler* [1973] and that the local change of heat content at such a midlatitude is nearly balanced with the net surface heat flux [*Yan et al.*, 1995]. The net surface heat flux (N) is calculated from daily NCEP/NCAR reanalysis data near the Korea and Tsugaru straits (Figure 1) and the temperature is averaged in the upper surface layer using climatological monthly temperature data of general digital environmental model (GDEM) [*Teague et al.*, 1990] nearest to the grid points of NCEP heat flux data. η_α outside each strait is estimated as

$$\eta_\alpha(t+1) = \frac{\varepsilon(t)N'(t)}{\rho_0 C_P}\Delta t + \eta_\alpha(t), \tag{11}$$

where $\varepsilon = \rho^{-1}\partial\rho/\partial T$ is the thermal expansion coefficient, N' $(= N - \overline{N})$ is the anomalous net surface heat flux from the temporal average $\overline{N}$, C_P is the specific heat of the seawater, and Δt is one day. The mean of η_α from 1998 to 2001 is removed to consider only variation parts and all the data are

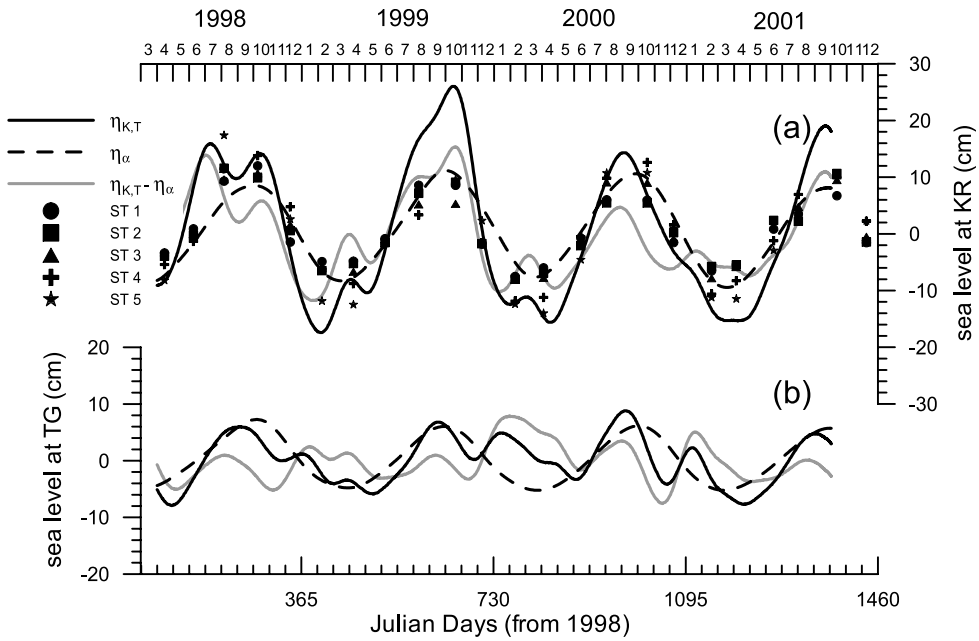

Figure 9. Sea levels outside the (a) Korea and (b) Tsugaru straits after low-pass filtering with a cutoff period of 90 days. The solid lines denote the adjusted sea levels observed ($\eta_{K,T}$) at (a) Sasebo and (b) Urakawa. Dashed lines are the steric sea level anomalies (η_α) outside each strait, which are estimated in the upper surface layer of 200 m according to the method suggested by *Stammer* [1997]. Shaded lines designate the corrected sea levels ($\eta_{K,T} - \eta_\alpha$). Symbols in Figure 9a denote the steric sea level anomalies calculated from bimonthly hydrographic data at each station of line 205 of KODC (Figure 1).

low-pass filtered with a cutoff period of 90 days. Estimated η_α shows clear seasonal variations with a maximum in September and a minimum in March and their ranges are about ±10 and ±5 cm outside the Korea and Tsugaru straits, respectively (Figure 9). Interannual variations in η_α are one order of magnitude smaller than seasonal variations.

[40] η_α estimated from the net surface heat flux at the Korea Strait is compared with the steric sea level anomaly (Figure 9a), which is calculated from bimonthly hydrographic data of line 205 of KODC (Figure 1) as follows.

$$\eta_\alpha = g^{-1} \int_{P_0}^{0} \Delta\alpha dp, \tag{12}$$

where $\Delta\alpha$ is the specific volume anomaly and P_0 is the bottom pressure at each station of line 205. Both kinds of η_α in the Korea Strait have similar time series with roughly the same variation range (Figure 9a). It implies that steric effects in sea levels can be estimated well from the net surface heat flux based on the simple assumption that the local change of heat content is nearly balanced with the net surface heat flux. These steric effects are removed from the adjusted sea levels observed at Sasebo (η_K) and Urakawa (η_T) (Figure 1). Steric sea level anomalies η_α account for 67 and 44% of total variances of η_K and η_T, respectively (Figures 9a and 9b). Therefore steric effects should be corrected before using the adjusted sea levels as forces to drive the strait flows in the simple barotropic model.

[41] Figure 10a is a stacked bar graph of the analytically reproduced transport through the Korea Strait. It shows that most seasonal to interannual variations in Q_K with a range of 1–2 Sv are forced mainly by η_K and η_T. $Q_K\_\eta_K$ and $Q_K\_\eta_T$ have variation ranges of ±0.8 and ±0.4 Sv, respectively. $Q_K\_\tau_{y\_K}$ makes a small contribution to the total variations of Q_K, whose range is about ±0.2 Sv. The magnitude of the sum of all the effects (Q_{K_all}) is comparable to that of Q_K and they are almost in phase with their correlation coefficient as high as 0.74 (Figure 11b). There seems to be a tendency that the transport becomes large in summer and autumn and small in winter and spring. However, interannual variations are so distinct that the seasonal variation is very weak from spring 2000 to spring 2001 (Figure 11b). This is caused mainly by relatively low η_K in summer and fall 2000 compared to that in other years (Figure 10a). Long-term variations in Q_{K_all} are nearly in phase with Q_{T_all} and their variation ranges are almost the same (Figures 11b and 11c). As in the subinertial and monthly variations (Figure 8d), Q_{S_all} has also very weak seasonal to interannual variations (Figure 11d).

[42] In contrast to Q_K, seasonal to interannual variations in η_0 are dominated by P_a and η_K (Figure 10b). $\eta_0\_P_a$ and $\eta_0\_\eta_K$ have variation ranges of about ±5 and ±7 cm, respectively. $\eta_0\_\eta_T$ makes a small contribution to the total variation of η_0, whose range is about ±2 cm. The magnitude of the sum of all the effects (η_{0_all}) is comparable to that of η_0 and they are almost in phase with their correlation coefficient as high as 0.92 (Figure 11a), where the steric effect in η_0 is also removed in the same way as applied to η_K and η_T. Seasonal variations in η_0 are prominent, whose range is about ±10 cm with a maximum in July and August and a minimum in December and January. The mean sea

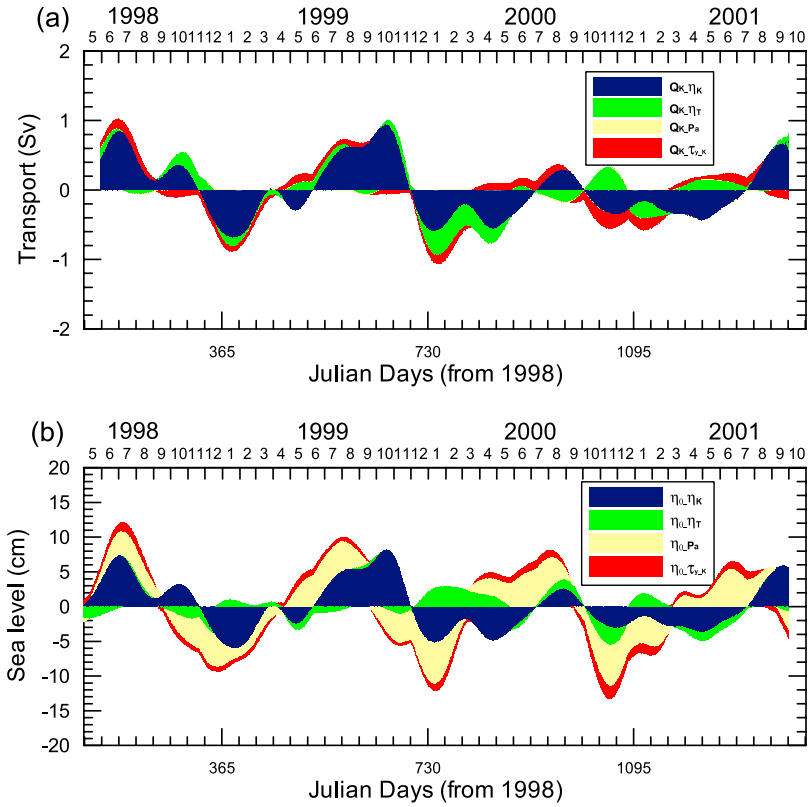

Figure 10. Stacked bar graph of (a) the transport through the Korea Strait and (b) the mean sea level of the East Sea, which are analytically reproduced by each force on the seasonal to interannual timescales.

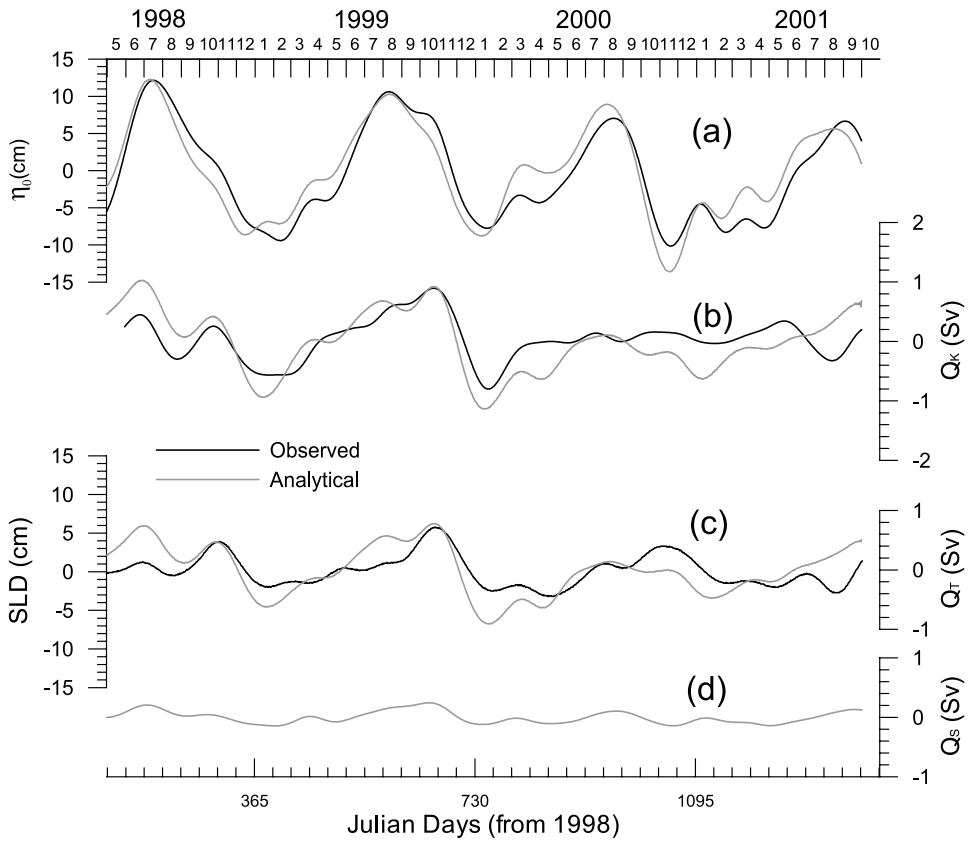

Figure 11. Same as in Figure 8 except for the seasonal to interannual timescales.

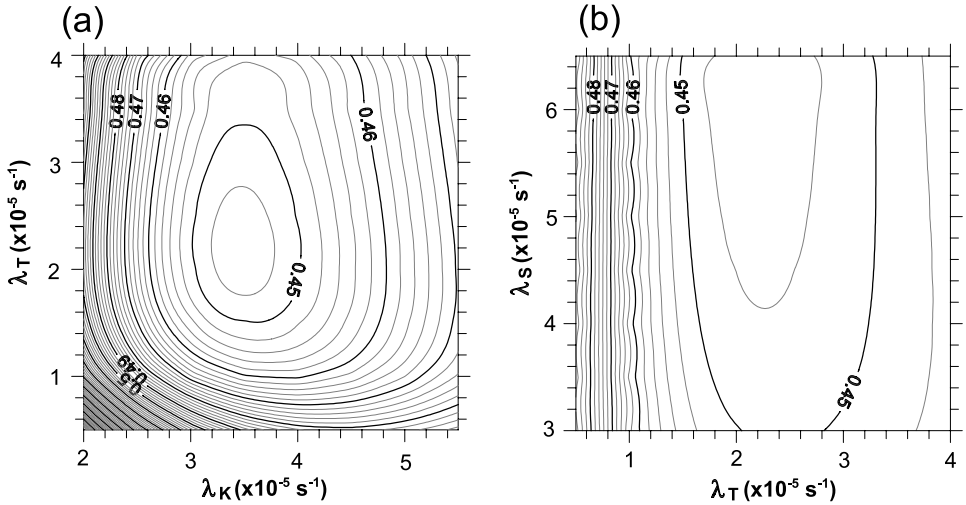

Figure 12. Variation in the RMS difference (in Sv) between the observed transport (Q_K) and the analytically reproduced transport (Q_{K_all}) through the Korea Strait according to friction coefficients at the three straits ($\lambda_{K,T,S}$). Here (a) λ_S fixed at 5.5×10^{-5} s^{-1} and (b) λ_K fixed at 3.5×10^{-5} s^{-1}. Contour interval is 0.002 Sv.

level in 2000 is lower than that in 1999 by 2.7 and 2.2 cm for η_0 and η_{0_all}, respectively. This results also from relatively low η_K in summer and fall 2000 compared to that in other years (Figure 10b).

5. Discussion

[43] In section 3 the friction at the strait was simply estimated on the assumption that it consists of the linearly parameterized bottom friction (λ_f) and the geostrophic control ($\lambda_g = fW/2L$). First, the two influences are compared by the ratio FG($= \lambda_f/\lambda_g = 2L\lambda_f/fW$) to examine whether the strait flow is more constrained by the bottom friction or by the geostrophic control. The last column in Table 1 shows the estimated value of FG at the three straits. While the bottom friction is a factor of 2 more important than the geosrophic control at the Tsugaru and Soya straits, the flow through the Korea Strait is more geostrophically controlled. However, *Ohshima* [1994] estimated this ratio FG about 0.1 at all the three straits and argued that the strait flows are geostrophically controlled. This difference results from the following factors. *Ohshima* [1994] did not consider the effect of the fast barotropic wave in a semienclosed basin [*Wright*, 1987], i.e., his formulation of the geostrophic control ($\lambda_g = fW/L$) is not divided by a factor of 2 as in this study. He used the smaller ratios of the strait length (L) to the strait width (W) at the Tsugaru and Soya straits as well as the smaller bottom frictional parameters at the three straits.

[44] However, it is not obvious to properly estimate the bottom friction in a linear form. Moreover, it is also uncertain to set the appropriate value of the along-strait length L (Table 1) in the estimation of the geostrophic control. We need therefore to assess how sensitively the previous results in section 3 and 4 depend on the selected friction coefficient λ. This sensitivity is measured in terms of the RMS difference between the voltage-derived transport (Q_K) and the analytically reproduced transport (Q_{K_all}) through the Korea Strait on the timescales of 2–60 days (Figure 12) even though Q_K can be affected by other forces not considered here. In Figure 12a the friction coefficient at the Soya Strait (λ_S) is fixed at 5.5×10^{-5} s^{-1} and the RMS difference is calculated for the possible ranges of the friction coefficients λ_K and λ_T. The RMS difference is much more sensitive to λ_K than λ_T because the vertical cross sectional area of the Korea Strait is larger than that of the Tsugaru Strait (Table 1). The minimum RMS difference is obtained for $\lambda_K = 3.5 \times 10^{-5}$ s^{-1} and $\lambda_T = 2.5 \times 10^{-5}$ s^{-1}. In Figure 12b the friction coefficient λ_K is fixed at 3.5×10^{-5} s^{-1}, and other two friction coefficients λ_S and λ_T are changed within their possible ranges. The RMS difference is more sensitive to λ_T than λ_S as expected. There is a trough along $\lambda_T = 2.5 \times 10^{-5}$ s^{-1} and the RMS difference varies very little with λ_S along this trough. The minimum RMS difference is obtained for $\lambda_T = 2.5 \times 10^{-5}$ s^{-1} and $\lambda_S = 5.5 \times 10^{-5}$ s^{-1}. The selected friction coefficients ($\lambda_K = 3.5 \times 10^{-5}$ s^{-1}, $\lambda_T = 2.5 \times 10^{-5}$ s^{-1}, $\lambda_S = 5.5 \times 10^{-5}$ s^{-1}), which give the minimum RMS difference of 0.45 Sv, are similar to the originally estimated friction coefficients ($\lambda_K = 2.7 \times 10^{-5}$ s^{-1}, $\lambda_T = 2.7 \times 10^{-5}$ s^{-1}, $\lambda_S = 5.6 \times 10^{-5}$ s^{-1}) in Table 1, which give the RMS difference of 0.46 Sv. This implies that the friction coefficients are reasonably estimated and the results are not so sensitive to them within their possible ranges.

[45] Even though the East Sea was assumed as a flat-bottomed basin in the analytical barotropic model for simplicity, in reality the continental shelves are developed inside the East Sea (Figure 1). The shelf waves (SWs) can be excited by the volume flux through the straits and they propagate in the same direction of the Kelvin waves [*Middleton and Viera*, 1991; *Ohshima*, 1994]. Since the phase speed of the SW is O(1 m/s) or less [*Middleton*, 1991], which is much less than that of the barotropic Kelvin wave, the SWs may not significantly modify the sea level distribution inside the East Sea at the subinertial periods and the assumption of the uniform sea level may remain valid. However, when the timescale gets longer, the SWs would be developed and propagate along the

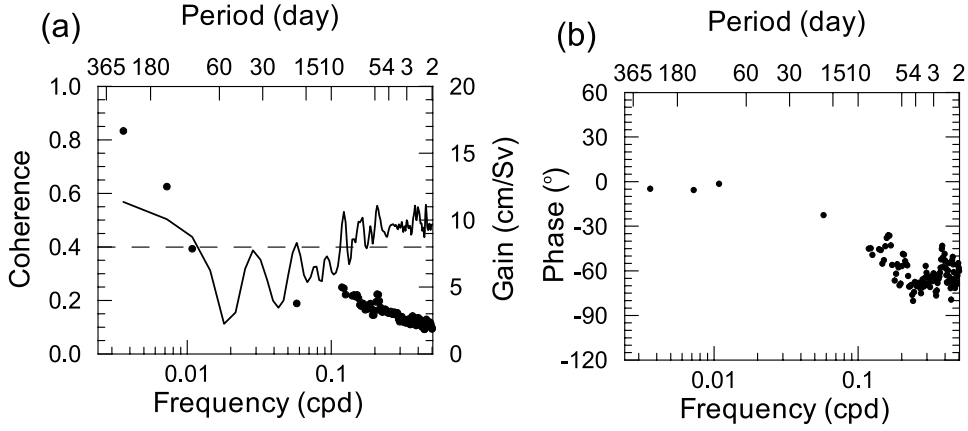

Figure 13. (a) Coherence (solid line), gain (dots), and (b) phase relation (dots) between the observed mean sea level of the East Sea (η_0) and the transport through the Korea Strait (Q_K). Gain and phase are plotted only when coherence is higher than the 95% confidence level (dashed line in Figure 13a).

adjacent shelves in the East Sea and a part of the sea level deviations would be carried by the SWs mainly over the continental shelves. The assumption made in the flat-bottomed basin therefore should be modified.

[46] Moreover, the wind stress, whose effects were neglected inside the East Sea due to its short horizontal length scale relative to the external Rossby radius of deformation, may induce the flows over the shallow shelves and then cause the flows through the straits. It may be related to the fact that the analytically obtained amplitude ratio (gain) between the transport through the Korea Strait (Q_K) and the along-strait wind stress at the Korea Strait (τ_{y_K}) (solid line in Figure 5c) is smaller than that obtained from the observed Q_K and τ_{y_K} (solid dots in Figure 5c) at long periods. It may also explain why the analytical model accounts for only about 50% of the total variance in the observed Q_K at the monthly periods in Figure 7a.

[47] We examine how the volume of the East Sea is changed by continuity (2). The gain and phase relations between the strait flows ($Q_{K,T,S}$) and the mean sea level (η_0) depend on the driving forces and the timescales as expected in Figure 5. If there is only the atmospheric pressure force to drive $Q_{K,T,S}$ and η_0, the strait flows into or out of the East Sea leads the mean sea level increase or decrease by continuity. Their phase differences are about 90° and the gain from $Q_{K,T,S}$ to η_0 generally increase with the timescale (Figures 5a and 5b). However, if other forces such as τ_{y_K}, η_K, and η_T drive $Q_{K,T,S}$ and η_0, the gain and phase relations between $Q_{K,T,S}$ and η_0 are dependent on the timescale. For example, Q_K driven by η_K leads η_0 by about 90° at short periods (Figure 5f) because all the inflow, Q_K, cannot simultaneously flow out of the basin through the Tsugaru and Soya straits due to the finite volume of the straits and the friction in the straits. At long periods a steady state will be reached at each strait by balancing between two forces (pressure gradient force and friction) and all the volume transport of Q_K can go out of the basin through other two straits and there is not an additional change in η_0 by continuity. $Q_{K,T,S}$ and η_0 therefore become all in phase (Figure 5f). The gain from Q_K to η_0 has a constant value of about 10 cm/Sv at long periods and it decreases at short periods (Figure 5e).

[48] Figure 13 shows the cross spectra between the observed η_0 and Q_K. Their coherence is higher than the 95% confidence level at the subinertial periods and the periods longer than 100 days (solid line in Figure 13a). Since η_0 and Q_K may be affected by all the forces (P_a, τ_{y_K}, η_K, and η_T), the gain and phase relations between η_0 and Q_K are the combined results depending on the relative importance among the forces and their phase relations. The phase difference between η_0 and Q_K increases from 30° to 90° (Figure 13b) and their gain decreases from 5 to 2 cm/Sv (dots in Figure 13a) at the subinertial periods. When the timescale gets longer, η_0 and Q_K become in phase and their gain has the values of 8–17 cm/Sv. These results are caused by the fact that P_a dominates the changes in η_0 and Q_K at the subinertial periods (Figure 7) while η_K and η_T becomes more important at longer periods (Figure 10). Note that even though P_a can cause about half part of the variations in η_0 at long periods (Figure 10b), the related volume transport through each strait is very small due to the long periods (Figure 10a) and hence the atmospheric pressure forced transport may contribute very little to the cross spectra between η_0 and Q_K in Figure 13.

[49] As manifested in the previous section, the mean sea level in the East Sea (η_0) has large subinertial (2–10 days) variations and they are mainly caused by the non-isostatic response to the atmospheric pressure. Since the repeat period of TOPEX/Poeidon or Jason is 10 days, these subinertial barotropic variations in the mean sea level of the East Sea (η_0) may be aliased into satellite altimetric data and contaminate longer timescale signals as reported in the Mediterranean [*Le Traon and Gauzelin*, 1997] and the global ocean [*Fukumori et al.*, 1998; *Stammer et al.*, 2000]. *Nam et al.* [2004] showed that nonisostatic responses of the sea level in the East Sea ($\eta_0\_P_a$) provide an improved correction of atmospheric pressure effects on TOPEX/Poseidon altimeter data by using the same analytical model as in this study but considering P_a only. Subinertial to monthly variations in η_0, however, are explained significantly more by this model considering other forces such as $\eta_{K,T}$ and τ_{y_K}. This model can be used to correct the remaining aliasing effects of very high frequency motions on satellite altimetric data in the East Sea. For

example, the sum of all the effects (η_{0_all}) accounts for 84% of the total variance of η_0 while $\eta_{0\_}P_a$ accounts only for 55% on the timescales of 2–60 days.

[50] We used the adjusted sea level variations outside the straits of the East Sea as driving forces without trying to find what originally drives them. The local along-coast wind stress can be considered as a potential factor. *Sandstorm* [1980] reported that the along-coast wind stress component (τ) piles the water up or down along the coast and that the expected sea level change (η) at the coast is given by

$$\eta \approx \frac{fL_{CS}}{g}\left(\frac{|\tau|}{\rho C_D}\right)^{1/2}, \tag{13}$$

where L_{cs} is the width of the continental shelf, C_D is a drag coefficient. *Garrett* [1983] suggested that the flows through the Strait of Gibraltar can be induced by the sea level change due to the along-coast, i.e., the cross-strait, wind stress outside the strait. Using (13) with L_{cs} of 100 km and C_D of 3.0×10^{-3}, the change of 0.02 N/m^2 in τ can cause the sea level change of about 8cm, which is the order of magnitude of the adjusted sea level changes outside the straits of the East Sea (Figure 9).

6. Conclusions

[51] Continuous measurement of cable voltage between Pusan, Korea and Hamada, Japan reveals large variability in the inflow through the Korea Strait on short-period subinertial to interannual timescales, which was not known previously. This finding raises an interesting question on the driving mechanisms of flows through straits of the East Sea. A simple analytical model is introduced to understand the barotropic responses in the East Sea. The East Sea is simplified as a semienclosed flat-bottomed basin connected with the open ocean through three shallow straits where flows are constrained by the linear friction and the geostrophic control at the periods longer than the inertial period. The flows through the straits are forced by the atmospheric pressure over the East Sea, the along-strait wind stress at the Korea Strait, and pressure differences along the straits, which are caused by the adjusted sea level changes outside the straits.

[52] Most variations in transports through the straits and the mean sea level of the East Sea can be reproduced using this simple model. This model shows that the response to the atmospheric pressure in the East Sea is nonisostatic at the subinertial periods of 2–10 days. The atmospheric pressure dominates the subinertial transport variations of 1–3 Sv with a maximum at the period of the Helmholtz resonance between the East Sea and the Pacific Ocean through the three straits. This period is estimated at about 3 days, which is related to the timescale for the basin to be filled or drained by the strait flows. The atmospheric pressure-driven flows into or out of the East Sea induce its mean sea level rise or drop with a range of 10–30 cm.

[53] While most variance in the mean sea level of the East Sea can be explained by its barotropic responses to the atmospheric pressure, a significant part of its monthly to interannual variations of 10–20 cm are also explained by the adjusted sea level changes outside the straits. The effects of the atmospheric pressure on transport variations become very weak at low frequencies because there is enough time for the strait flows to fill and drain the East Sea as its mean sea level responds isostatically. On the other hand, the changes in the adjusted sea levels outside the straits cause the pressure gradient forces at the straits and play dominant roles in the transport variations of 1–2 Sv at the monthly to interannual periods. The strait flows and the mean sea level become all in phase at these long periods because the pressure gradient force is balanced by the friction at each strait and a steady state is reached.

[54] The analytical model in this study, however, is too simple to account for the effects of the topographic change, stratification, wind stress curl, heat flux, and nonlinearity. A numerical model with more realistic representation of the ocean can be surely used to understand further the driving mechanisms of variations in the strait flows and the mean sea level of the East Sea. As relevant timescales get longer, nonlocal effects such as remotely propagated baroclinic waves will play important roles and hence the East Sea should be considered as a part of the large system instead of a local system.

[55] **Acknowledgments.** We thank two reviewers for their valuable comments. This work was granted by the Korea Research Foundation, South Korea, through the BK21 Project and the Basic Research Promotion (KRF-2005-070-C00142).

References

Blaha, J., and R. Reed (1982), Fluctuations of sea level in the western North Pacific and inferred flow of the Kuroshio, *J. Phys. Oceanogr.*, *12*, 669–678.

Candela, J., C. D. Winant, and H. Bryden (1989), Meteorologically forced subinertial flows through the Strait of Gibraltar, *J. Geophys. Res.*, *94*, 12,667–12,679.

Cho, Y. K., and K. Kim (2000), Branching mechanism of the Tsushima Current in the Korea Strait, *J. Phys. Oceanogr.*, *30*, 2788–2797.

Csanady, G. T. (1982), *Circulation in the Coastal Ocean*, 279 pp., Springer, New York.

Emery, W. J., and R. E. Thomson (1998), *Data Analysis Methods in Physical Oceanography*, 634 pp., Elsevier, New York.

Fukumori, I., R. Raghunath, and L.-L. Fu (1998), Nature of global large-scale sea level variability in relation to atmospheric forcing: A modeling study, *J. Geophys. Res.*, *103*, 5493–5512.

Garrett, C. (1983), Variable sea level and strait flows in the Mediterranean: A theoretical study of the response to meteorological forcing, *Oceanol. Acta*, *6*, 79–87.

Garrett, C., and F. Majaess (1984), Non-isostatic response of sea level to atmospheric pressure in the eastern Mediterranean, *J. Phys. Oceanogr.*, *14*, 656–665.

Gill, A. E., and P. P. Niiler (1973), The theory of the seasonal variability in the ocean, *Deep Sea Res.*, *20*, 141–177.

Hannah, C. G. (1992), Geostrophic control with wind forcing: Application to Bass Strait, *J. Phys. Oceanogr.*, *22*, 1596–1599.

Ichikawa, H., and R. C. Beardsley (1993), Temporal and spatial variability of volume transport of the Kuroshio in the East China Sea, *Deep Sea Res., Part I*, *40*, 583–605.

Isobe, A., and S. Imawaki (2002), Annual variation of the Kuroshio transport in a two-layer numerical model with a ridge, *J. Phys. Oceanogr.*, *32*, 994–1009.

Isobe, A., S. Tawara, A. Kaneko, and M. Kawano (1994), Seasonal variability in the Tsushima Warm Current, Tsushima-Korea Strait, *Cont. Shelf Res.*, *14*, 23–35.

Kim, K., S. J. Lyu, Y.-G. Kim, B. H. Choi, K. Taira, H. T. Perkins, W. J. Teague, and J. W. Book (2004), Monitoring volume transport through measurement of cable voltage across the Korea Strait, *J. Atmos. Oceanic Technol.*, *21*, 671–682.

Kubota, M., H. Yokota, and T. Okamoto (1995), Mechanism of the seasonal transport variation through the Tokara Strait, *J. Oceanogr.*, *51*, 441–458.

Lee, D.-K., P. P. Niiler, S.-R. Lee, K. Kim, and H.-J. Lie (2000), Energetics of the surface circulation of the Japan/East Sea, *J. Geophys. Res.*, *105*, 19,561–19,573.

Lee, T. N., and E. J. Williams (1988), Wind forced transport fluctuations of the Florida Current, *J. Phys. Oceanogr.*, *18*, 937–946.

Lee, T. N., W. E. Johns, C.-T. Liu, D. Zhang, R. Zantopp, and Y. Yang (2001), Mean transport and seasonal cycle of the Kuroshio east of Taiwan with comparison to the Florida Current, *J. Geophys. Res.*, *106*, 22,143–22,158.

Le Traon, P.-Y., and P. Gauzelin (1997), Response of the Mediterranean mean sea level to atmospheric pressure forcing, *J. Geophys. Res.*, *102*, 973–984.

Lyu, S. J., and K. Kim (2003), Absolute transport from the sea level difference across the Korea Strait, *Geophys. Res. Lett.*, *30*(6), 1285, doi:10.1029/2002GL016233.

Lyu, S. J., K. Kim, and H. T. Perkins (2002), Atmospheric pressure-forced subinertial variations in the transport through the Korea Strait, *Geophys. Res. Lett.*, *29*(9), 1294, doi:10.1029/2001GL014366.

Middleton, J. F. (1991), Coastal-trapped wave scattering into and out of straits and bays, *J. Phys. Oceanogr.*, *21*, 681–694.

Middleton, J. F., and F. Viera (1991), The forcing of low frequency motions within Bass Strait, *J. Phys. Oceanogr.*, *21*, 695–708.

Minato, S., and R. Kimura (1980), Volume transport of the western boundary current penetrating into a marginal sea, *J. Oceanogr. Soc. Jpn.*, *36*, 185–195.

Mizuno, S., K. Kawatate, T. Nagahama, and T. Miita (1989), Measurements of East Tsushima current in winter and estimation of its seasonal variability, *J. Oceanogr. Soc. Jpn.*, *45*, 375–384.

Moriyasu, S. (1972), The Tsushima Current, in *Kuroshio*, edited by H. Stommel and K. Yoshida, pp. 353–369, Univ. of Tokyo Press, Tokyo.

Nam, S. H., S. J. Lyu, Y. H. Kim, K. Kim, J.-H. Park, and D. R. Watts (2004), Correction of TOPEX/Poseidon altimeter data for nonisostatic sea level response to atmospheric pressure in the Japan/East Sea, *Geophys. Res. Lett.*, *31*, L02304, doi:10.1029/2003GL018487.

Nof, D. (1993), The penetration of Kuroshio water into the Sea of Japan, *J. Phys. Oceanogr.*, *23*, 797–807.

Nof, D. (2000), Why much of the Atlantic circulation enters the Caribbean Sea and very little of the Pacific circulation enters the Sea of Japan, *Prog. Oceanogr.*, *45*, 39–67.

Ohshima, K. I. (1994), The flow system in the Japan Sea caused by sea level difference through shallow straits, *J. Geophys. Res.*, *99*, 9925–9940.

Otnes, R. K., and L. Enochson (1972), *Digital Time Series Analysis*, 467 pp., John Wiley, Hoboken, N. J.

Park, J.-H., and D. R. Watts (2005), Response of the southwestern Japan/East Sea to atmospheric pressure, *Deep Sea Res., Part II*, *52*, 1671–1683.

Sandstorm, H. (1980), On the wind-induced sea level changes on the Scotian Shelf, *J. Geophys. Res.*, *85*, 461–468.

Schott, F., T. N. Lee, and R. Zantopp (1988), Variability of structure and transport of the Florida Current in the period range of days to seasonal, *J. Phys. Oceanogr.*, *18*, 1209–1230.

Stammer, D. (1997), Steric and wind-induced changes in TOPEX/Poseidon large-scale sea surface topography observations, *J. Geophys. Res.*, *102*, 20,987–21,009.

Stammer, D., C. Wunsch, and R. M. Ponte (2000), De-aliasing of global high frequency barotropic motions in altimeter observations, *Geophys. Res. Lett.*, *27*, 1175–1178.

Takikawa, T., J.-H. Yoon, and K.-D. Cho (2005), The Tsushima Warm Current through Tsushima straits estimated from ferryboat ADCP data, *J. Phys. Oceanogr.*, *35*, 1154–1168.

Teague, W. J., M. J. Carron, and P. J. Hogan (1990), A comparison between the generalized digital environmental model and Levitus climatologies, *J. Geophys. Res.*, *95*, 7167–7183.

Teague, W. J., G. A. Jacobs, H. T. Perkins, J. W. Book, K.-I. Chang, and M.-S. Suk (2002), Low frequency current observations in the Korea Strait, *J. Phys. Oceanogr.*, *32*, 1621–1641.

Toba, Y., K. Tomizawa, Y. Kurasawa, and K. Hanawa (1982), Seasonal and year-to-year variability of the Tsushima–Tsugaru Warm Current system with its possible cause, *Mer*, *20*, 41–51.

Toulany, B., and C. Garrett (1984), Geostrophic control of fluctuating barotropic flow through straits, *J. Phys. Oceanogr.*, *14*, 649–655.

Wright, D. G. (1987), Comments on "Geostrophic control of fluctuating barotropic flow through straits," *J. Phys. Oceanogr.*, *17*, 2375–2377.

Yan, X.-H., P. P. Niiler, S. K. Nadiga, R. H. Stewart, and D. R. Cayan (1995), Seasonal heat storage in the North Pacific: 1976–1989, *J. Geophys. Res.*, *100*, 6899–6926.

Yi, S. U. (1966), Seasonal and secular variations of the water volume transport across the Korea Strait, *J. Oceanol. Soc. Korea*, *1*, 7–13.

K. Kim, School of Earth and Environmental Science, Room 25-1-317, Seoul National University, San 56-1, Silim-dong, Kwanak-gu, Seoul 151-742, South Korea.

S. J. Lyu, Department of Oceanography, Chonnam National University, Kwangju 500-757, South Korea. (sjlyu@ocean.snu.ac.kr)